SCIENCE CHINA
Information Sciences

• RESEARCH PAPER •

January 2026, Vol. 69, Iss. 1, 112401:1–112401:10
https://doi.org/10.1007/s11432-025-4505-1

Ambipolar MoS_2 enabled through high-ε ferroelectric P(VDF-TrFE)

Zhaobiao DIAO[1,2†], Shuaiqin WU[1,3†], Yan CHEN[1,3*], Lu WANG[1,2], Chang LIU[1], Binmin WU[1], Peng WANG[1], Tie LIN[1,5], Hong SHEN[1,5*], Xiangjian MENG[1,5], Xudong WANG[1,5*], Junhao CHU[1,3] & Jianlu WANG[1,3,4]

[1]*State Key Laboratory of Infrared Physics, Shanghai Institute of Technical Physics, Chinese Academy of Sciences, Shanghai 200083, China*
[2]*University of Chinese Academy of Sciences, Beijing 100049, China*
[3]*Shanghai Frontiers Science Research Base of Intelligent Optoelectronics and Perception, Institute of Optoelectronics, Fudan University, Shanghai 200433, China*
[4]*Frontier Institute of Chip and System, Fudan University, Shanghai 200433, China*
[5]*Shanghai Key Laboratory of Optical Coatings and Spectral Modulation, Shanghai Institute of Technical Physics, Chinese Academy of Sciences, Shanghai 200083, China*

Received 21 February 2025/Revised 12 May 2025/Accepted 20 June 2025/Published online 4 January 2026

Abstract The p-type and n-type transistors are the basic components for building CMOS electronic devices for logic circuits. Most two-dimensional materials are n-type due to strong electron doping by intrinsic structural defects. Notably, the p-type conductivity of MoS_2 is hardly achievable by the limited electric field modulation from the low dielectric constant of Si/SiO_2. However, through strong dielectric screening of a high dielectric constant substrate and powerful polarization electric field of ferroelectric material, the p-type transition of MoS_2 can be realized. In this paper, with the help of ferroelectric field modulation of high dielectric constant P(VDF-TrFE), a significant modulation of the band structure of MoS_2 is realized, and finally, a flexible p-type modulation of MoS_2 is obtained. The band changes and electrical properties of MoS_2 on three different dielectric constant substrates, including Si/SiO_2, hBN, and P(VDF-TrFE), were quantitatively studied with Kelvin probe force microscopy (KPFM). Fermi level changes and band n-p transitions of MoS_2 under ferroelectric modulation were also systematically investigated by KPFM. The ferroelectric modulation of the MoS_2 Fermi level can realize a wide range of flexible modulation up to nearly 900 meV. This work reveals the device physics of the realization of p-type transport from the band perspective and provides an effective and viable reference for p-type modulation of other two-dimensional materials. It also provides a boost for the application of MoS_2 in high-performance electronic and optoelectronic devices.

Keywords p-type semiconductor, dielectric constant, ferroelectric modulation, MoS_2, AFM

Citation Diao Z B, Wu S Q, Chen Y, et al. Ambipolar MoS_2 enabled through high-ε ferroelectric P(VDF-TrFE). Sci China Inf Sci, 2026, 69(1): 112401, https://doi.org/10.1007/s11432-025-4505-1

1 Introduction

In the face of the increasing demand for device miniaturization, the development of novel channel materials has received focused attention from researchers. Low-dimensional materials are considered the key solution to continuing Moore's law. Two-dimensional materials, represented by graphene [1], BP [2,3], and transition-metal dichalcogenides (TMDs) [4,5], have been widely studied and applied in the fields of nanoelectronic devices, optoelectronic sensing, and logic electronics [6–13]. Most 2D semiconductors are n-type due to strong electron doping by interfacial defects and intrinsic structural defects. Only a small part of the few p-type semiconductors meet the requirements of high mobility and stability applications, such as BP [14], b-AsP [15], and WSe_2 [16]. P-type semiconductors are an indispensable part of the composition of CMOS devices and play a crucial role in many electronic and optoelectronic devices, such as complementary logic circuits, phototransistors, and light-emitting diodes. P-type two-dimensional materials are important components of functional van der Waals heterostructures (VDWHs). By integrating p-type semiconductors with different 2D materials, complex integrated optoelectronic devices can be constructed and excellent device performance can be achieved. However, the lack of p-type materials limits the integration of 2D materials for nanoelectronics applications.

* Corresponding author (email: yanchen_@fudan.edu.cn, Hongshen@mail.sitp.ac.cn, wxd0130@mail.sitp.ac.cn)
† These authors contributed equally to this work.

Therefore, researchers look at transforming n-type semiconductors into p-type semiconductors through direct synthesis or artificial doping. The three main approaches currently include contact engineering, chemical doping, and electrostatic doping. Due to the ultra-thin thickness, the electronic properties of 2D materials are highly sensitive to external factors (electric field, dielectric environment, etc.) [17–19]. Therefore, the manipulation of the band structure, carrier density, or polarity of the material can be realized by using the electric field effect of the metal-insulator-semiconductor structure, which is the principle of electrostatic doping. Electrostatic doping overcomes the problems of lattice structure disruption and scattering of defects associated with chemical doping while enabling flexible and continuous modulation.

In particular, the doping of 2D materials by electric field originates from the band bending of the capacitive coupling between the gate electrode and 2D materials [20–22], which is mainly realized by the electric field effect of the metal-insulator-semiconductor structure. Under the effect of the gate electric field, polarized charges are generated on the upper and lower surfaces of the gate dielectric. Through Coulombic interaction, the polarized charges will attract or repel carriers inside the 2D material at the interface, thus forming a charge accumulation or depletion layer within the material, which in turn affects the material transport properties. MoS_2, as a typical TMD material with a layer-dependent bandgap, is one of the most mature materials in TMDs. MoS_2 exhibits n-type intrinsic properties due to environmental doping from surface adsorption/supporting substrate and electronic doping from sulfur vacancies. However, p-type MoS_2 lacks robust means of electrostatic doping. It has been shown that although the carrier concentration can be effectively manipulated using solid gate dielectrics such as SiO_2 and HfO_2, the inferior dielectric breakdown strength limits the modulation of carrier polarity [4, 23, 24]. MoS_2 p-type transition cannot be achieved by the SiO_2 gate electric field alone. In contrast, ferroelectric materials can achieve effective modulation of carrier concentration and polarity thanks to strong dielectric screening, high polarization field strength, and non-volatile and reconfigurable strong doping. Therefore, we chose the organic ferroelectric poly(vinylidene fluoride-trifluoroethylene) (P(VDF-TrFE)) thin film [25–30], which has large residual polarization and good thermal stability, to modulate MoS_2 to achieve p-type MoS_2 and probe the transition mechanism and transport behavior.

In this study, we first quantitatively compared the effects of three different dielectric environments, Si/SiO_2, hBN, and P(VDF-TrFE), on the band structure and electrical characteristics of MoS_2 by KPFM. Then we systematically investigated the bipolar behavior and band changes of MoS_2 under the P(VDF-TrFE) ferroelectric field modulation using in situ KPFM, revealing the changes of its Fermi level shift with the gate voltage. Finally, we directly investigated the flexible n-p transition in the band of MoS_2 homojunction under ferroelectric field modulation by combining in situ KPFM and scanning capacitance microscopy (SCM). The p-type modulation of MoS_2 under the ferroelectric field was also explained. The results show that under P(VDF-TrFE) ferroelectric field modulation, monopolar n-type MoS_2 realizes the p-type transition and exhibits bipolar properties. The Fermi level shifts significantly between the conduction and valence bands up to about 900 meV. Significant modulation of MoS_2 band structure by the strong dielectric screening and powerful ferroelectric polarization of high dielectric constant P(VDF-TrFE) is why MoS_2 is capable of flexible transition between n-p. This result provides an additional approach to MoS_2 p-type modulation and deepens the understanding of device physics. It is adaptable to other 2D materials and provides a referential method and theoretical reference for the development of p-type materials.

2 Methods

2.1 Device fabrication

For MoS_2 FETs, hBN was first mechanically exfoliated on a 285 nm SiO_2 substrate. Then few-layer MoS_2 was mechanically exfoliated and transferred by PDMS to the flat edge of the hBN sheet so that half of the MoS_2 was on SiO_2. Finally, Cr/Au electrodes (5/15 nm) were deposited by electron-beam lithography and thermal evaporation. The fabrication process of the MoS_2 FeFE is shown in Figure S1. First, the bottom electrode was deposited on the SiO_2 substrate. Then, P(VDF-TrFE) organic ferroelectric polymer solution was spin-coated and annealed in an oven at 135°C for 6 h. The thickness of the P(VDF-TrFE) film was about 300 nm. After that, MoS_2 was mechanically exfoliated and transferred to P(VDF-TrFE). Finally, the 50 nm Au source and drain electrodes deposited on the Si substrate were transferred to P(VDF-TrFE) by PVA and soaked in deionized water for 2 h to remove PVA.

2.2 Measurements

Electrical measurements were taken by an MStarter 200 photoelectric measurement system from Maita Photonics Technology Co., LTD. KPFM was done by an Asylum Research Cypher S series AFM from Oxford Instruments

under ambient conditions. A hard probe was used to clean the sample surface before testing. Tests were performed in nap mode using Si cantilevers with Ti/Ir coating. Source and drain electrodes were grounded during testing. The gate voltage was provided by an external Keithley 2400 series digital source meter. SCM was also performed by this AFM. It utilized a Pt probe and measured in contact mode. The probe was kept virtually grounded, and voltage was applied to the sample. The capacitance signal was scanned during the test.

3 Results and discussion

Before studying the regulation of MoS_2 by the P(VDF-TrFE) ferroelectric field, we first need to investigate the band structure of MoS_2 on the P(VDF-TrFE) substrate. Atomically thin materials are extremely sensitive to the surrounding dielectric environment due to their quasi-two-dimensional size. The strength of the Coulomb interaction between charge carriers originating from the weak dielectric screening in the two-dimensional limit is remarkably strong, leading to a reformulation of the electronic energy level with a change in the exciton binding energy [17]. Thus, the electronic bandgap, consisting of the optical bandgap and exciton binding energy, is also sensitive to the local dielectric environment. We have exfoliated different layers of MoS_2 on Si/SiO_2 substrates with a low dielectric constant ($\varepsilon = 3.9$) [31] and spin-coated P(VDF-TrFE) substrates with a high dielectric constant ($\varepsilon = 54$) [25] respectively. Theoretical calculations have shown that a high dielectric constant substrate introduces a higher degree of renormalization of the electronic bandgap, resulting in smaller MoS_2 exciton binding energy and quasiparticle bandgap [32]. As shown in Figure 1(a), the electronic energy level of MoS_2 on the P(VDF-TrFE) substrate is compressed compared to that on the Si/SiO_2 substrate.

Kelvin probe force microscopy was hired to measure the local surface potential of MoS_2 on both substrates. The top panels of Figures 1(b) and (c) show the surface potential maps of the same MoS_2 on Si/SiO_2 and P(VDF-TrFE) substrates, respectively. The bottom inset shows the topographic scanned by an atomic force microscope (AFM) and the edge height profile of MoS_2 on a Si/SiO_2 substrate. The thickness of around 3.5 nm confirms that this sample is composed of five layers. The bottom figures show the distribution of the contact potential difference (CPD) between MoS_2 and the conducting probe extracted along the red line in the surface potential images. Here, the contact potential difference is defined as the difference in the local work function between the KPFM tip and the sample:

$$\mathrm{CPD} = W_{\mathrm{tip}} - W_{\mathrm{sample}}, \tag{1}$$

where W_{tip} and W_{sample} are the average work functions of the tip and sample, respectively. The CPD of MoS_2 on the Si/SiO_2 substrate is -371 meV, while it is -500 meV on the P(VDF-TrFE) substrate. So it can be seen that the work function of MoS_2 on the P(VDF-TrFE) substrate is higher than that of the Si/SiO_2 substrate by 129 meV. In the test, we used probes with the same coating, so the change in CPD value reflected the shift of the Fermi level of MoS_2. This result proves that the MoS_2 on the high dielectric constant substrate shows a higher work function. The top panels of Figures 1(d) and (e) show the electron-hole Coulomb interaction of excitons in MoS_2 on both substrates, where the excitons are confined in the MoS_2 layer but the electric field between the electrons and holes of excitons crosses the material into the surrounding dielectric environment. According to the environmentally-sensitive theory of electronic and optical transitions in two-dimensional semiconductors, the screening ability of the high dielectric constant substrate for electron-hole separations is enhanced and the strength of the Coulomb interaction is simultaneously weakened, leading to a decrease in the exciton binding energy and the quasiparticle bandgap [17, 32]. The dependence of CPD on thickness calculated from the KPFM potential mappings of MoS_2 of different thicknesses on both substrates demonstrates in more detail the modification of the band structure of MoS_2 by the dielectric environment, as shown in the bottom panels of Figures 1(d) and (e). MoS_2 on the high dielectric constant substrate has a higher work function. And the thin-layer MoS_2 has a higher work function in comparison. The work function of MoS_2 shows a decreasing trend with increasing thickness. While, the CPD results on the Si/SiO_2 substrate show that the work function shift has a saturating trend after reaching a certain thickness (about 12.6 nm), which matches the theoretical calculation [33]. In this, we chose the point at the thickness where the Fermi level is shifted downward from the thinnest layer in the test by an amount reaching 90% of the total shift (Fermi level shift from the thinnest to the thickest layer of MoS_2 in the test) as the saturation point. This value is given by taking the results of the e-exponential fit to the data. The value is about 9.8 nm on the P(VDF-TrFE) substrate.

The band structure of materials is directly related to the electrical properties of devices, so we further investigated the effect of the dielectric environment on the electrical characteristics of MoS_2 field-effect transistors. We mechanically exfoliated multiple-layer hBN on a Si/SiO_2 substrate and transferred a five-layer MoS_2 to the hBN boundary, with a segment on low dielectric constant SiO_2 and a segment on high dielectric constant hBN ($\varepsilon =$

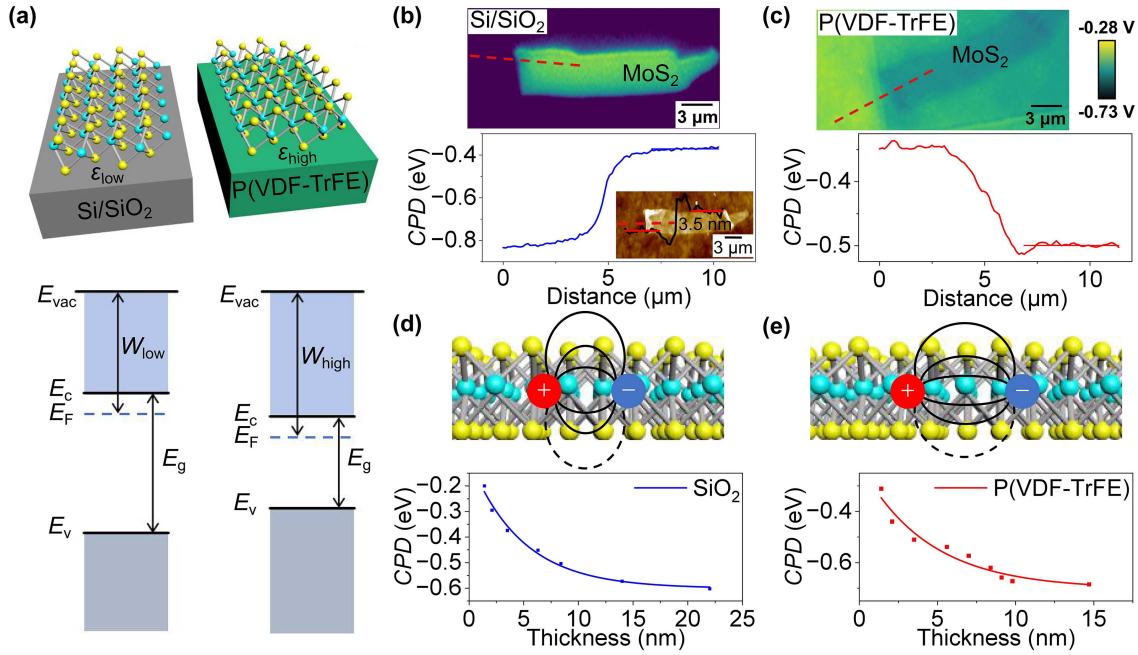

Figure 1 (Color online) Effect of dielectric environment on the band structure of MoS_2. (a) Schematic illustration and the expected band structure of MoS_2 exfoliated on a low dielectric constant substrate (Si/SiO_2) versus high dielectric constant (P(VDF-TrFE)). The dielectric environment affects the exciton binding energy and the electronic quasiparticle bandgap in 2D materials. The high dielectric constant substrate leads to a decrease in exciton binding energy due to stronger dielectric screening, resulting in a decrease in the MoS_2 bandgap. Results of surface potential measurements of five layers MoS_2 on Si/SiO_2 (b) and P(VDF-TrFE) (c) by KPFM. The top panels show the surface potential mappings of MoS_2. The bottom panels show the contact potential difference profile extracted along the red dashed line in the top figures. The inset in (b) shows the AFM morphology of MoS_2 and the corresponding height profile along the red line in the AFM mapping. The scale bars of the figures are all 3 μm. (d) and (e) Changes in band structure of MoS_2 with different thicknesses on different dielectric constant substrates. The top panels show the schematic illustration of the Coulomb interaction between the bound electron-hole in excitons in MoS_2 on Si/SiO_2 and P(VDF-TrFE) substrates. The strength of the Coulomb interaction between charged particles is reduced on the P(VDF-TrFE) substrate, leading to a decrease in both the exciton binding energy and the bandgap. The contact potential difference data show that MoS_2 on the P(VDF-TrFE) substrate has a lower Fermi level. The bottom panels show the dependence of the contact potential difference of MoS_2 on material thickness on two substrates. The Fermi level decreases rapidly with MoS_2 thickness and tends to saturate.

5.97) [31], respectively. Then, Cr/Au source-drain electrodes were deposited to form field effect transistors (FETs). The utilization of a single MoS_2 to fabricate both devices also eliminates the differences between devices caused by different MoS_2. Schematic diagrams and optical images of the two transistors are shown in Figures 2(a) and (d), and insets of Figures 2(b) and (e), respectively. Both devices show typical n-type behavior in their transfer characteristics, with better performance on hBN substrates, as shown in Figures 2(b) and (e). MoS_2 channel is n-type due to electron doping of sulfur vacancies [34]. The device conducts under positive gate voltage, which originates from the accumulation of electrons as channel majority carriers arising from the dielectric polarization charge. The device cuts off at a negative gate voltage, which originates from the depletion of channel electrons. We grounded the source and drain electrodes of the device and performed KPFM surface potential measurements at zero gate voltage. By extracting the CPD difference between MoS_2 and Au electrodes in the potential mappings, we calculate the position of MoS_2 Fermi level using Au as a reference to extract the material band information ($CPD_{MoS_2} - CPD_{Au} = W_{Au} - W_{MoS_2}$). The results show that the MoS_2 Fermi level on hBN is lower than that on Si/SiO_2 by 60 meV (Figures 2(c) and (f)), which is consistent with the results in Figures 1(b) and (c).

Despite the Fermi level shifting downward under negative gate voltage, the device still fails to achieve hole accumulation, which stems from the limited modulation due to the low dielectric constant of SiO_2. For MoS_2 FET on Si/SiO_2 substrate, p-type transport is extremely difficult to realize due to the large Schottky barrier height (SBH) of hole injection into the valence band caused by Cr/Au electrode work function limitation, coupled with the obstruction of the Fermi level pinning (FLP) of the metal/semiconductor interface near the conduction band [35, 36]. Meanwhile, interfacial charge adsorption from defects in the SiO_2 interface, polymer residues, and surface adsorbates such as water and oxygen [37] also has an impact on the p-type conductivity of MoS_2. Good linearity of the device output characteristic demonstrates the basic elimination of the FLP phenomenon (see Figure S1(a)). However, it is still impossible to achieve p-type MoS_2 with the SiO_2 gate-polarized electric field in this case. Theoretical calculations indicate that p-type modulation of MoS_2 requires a strong electric field [38]. Due to its low dielectric constant, the dielectric breakdown strength of the SiO_2 gate dielectric is low, which prevents the

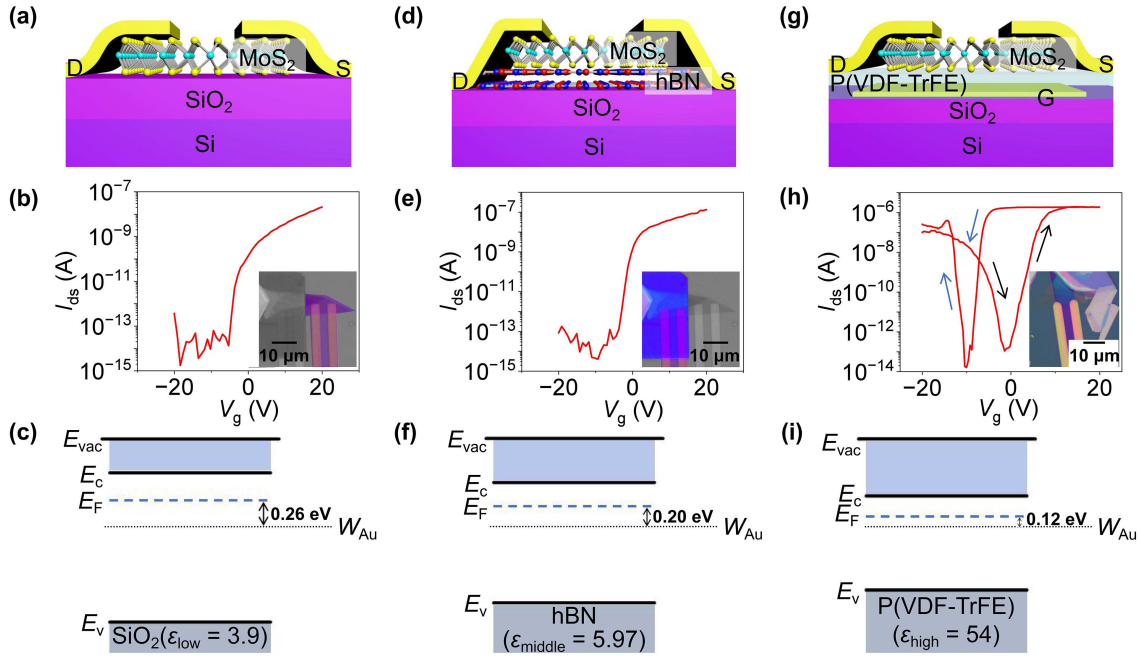

Figure 2 (Color online) Effect of dielectric environment on the electrical characteristics of MoS_2. (a) Schematic diagram of MoS_2 field effect transistor on Si/SiO_2 substrate. The device is composed of the SiO_2 gate dielectric and five-layer MoS_2 with Cr/Au source-drain contact. (b) Transfer characteristics of FET with the fixed source-drain voltage (V_{ds} = 1 V). The transfer characteristics exhibit typical n-type behavior. The inset is an optical image of the device, with the colored areas indicating the device regions. (c) Schematic diagram of the band extracted from the KPFM measurement at zero gate voltage. The source-drain Au electrode is grounded as a reference during the measurement, and the CPD difference between MoS_2 and Au electrode is calculated to extract the band information of MoS_2. The blue dashed line represents the Fermi level of MoS_2, and the black dashed line represents the position of the work function of Au. (d) Schematic diagram of MoS_2 field effect transistor on hBN substrate. The device is composed of the SiO_2 gate dielectric, underlying hBN, and five-layer MoS_2 with Cr/Au source-drain contact. (e) Transfer characteristics of FET with the fixed source-drain voltage (V_{ds} = 1 V). The transfer characteristics exhibit better performance compared to those on SiO_2. The inset is an optical image of the device, with the colored areas indicating the device regions. (f) Schematic diagram of the band extracted from the KPFM measurement at zero gate voltage. (g) Schematic diagram of MoS_2 ferroelectric field effect transistor with P(VDF-TrFE) bottom gate. The device is composed of a Cr/Au bottom electrode, P(VDF-TrFE) gate dielectric, and five-layer MoS_2 with Cr/Au source-drain contact. (h) The transfer characteristics exhibit n-type and p-type behaviors at positive and negative gate voltages, respectively, showing typical bipolar behavior. The arrows represent the gate voltage sweeping sequence. The inset is an optical image of the whole device. (i) Schematic diagram of the band extracted from the KPFM measurement at zero gate voltage.

realization of an electric field that can effectively modulate MoS_2. The limited modulation of the Fermi level leads to the hard realization of the accumulation of holes. It is also the same for hBN substrates, although hBN provides a good and flat interface with fewer defects.

Further, we deposited Cr/Au electrodes on the Si/SiO_2 substrate and spin-coated P(VDF-TrFE) as the bottom gate. Then a five-layer MoS_2 and Au electrodes were transferred to fabricate the back-gated MoS_2 ferroelectric field effect transistor (FeFET) (see Section 2 and Figure S2 for more details), as shown in Figure 2(g) and the inset in Figure 2(h). The transfer characteristic shows that the device achieves normal conduction at both positive and negative gate voltages, which indicates that carriers of MoS_2 achieve efficient switching of electrons and holes at different gate voltages, exhibiting n-type and p-type behavior, respectively (Figure 2(h)). The device exhibits typical bipolar behavior, which originates from the accumulation of electrons and holes in the MoS_2 channel achieved by the P(VDF-TrFE) ferroelectric field.

MoS_2 on P(VDF-TrFE) is collectively affected by ferroelectric polarization, interfacial charge trap states, and surface adsorption. Good output characteristic indicates that the transferred electrode provides good contact (see Figure S1(c)). The hysteresis direction of the transfer characteristic curve matches the direction of the P(VDF-TrFE) phase-voltage hysteresis loop (opposite to the hysteresis due to interfacial charge in the MoS_2 FET device on Si/SiO_2) (see Figure S1(c)), which suggests a significant reduction of the defect states at the semiconductor/(PVDF-TrFE) organic interface [39,40]. Thus, the MoS_2 state is essentially determined by the ferroelectric field. The same KPFM measurement shows a significant shift in the Fermi level of MoS_2 on P(VDF-TrFE) with a higher dielectric constant in comparison (Figure 2(i)). It also proves that the higher the dielectric constant, the larger shift in the Fermi level occurs. High dielectric screening due to high dielectric constant leading to significant compression of the MoS_2 bandgap by several hundred meV has also been reported [41]. According to the environmentally-sensitive theory of electronic and optical transitions in two-dimensional semiconductors [32], the enhancement of substrate

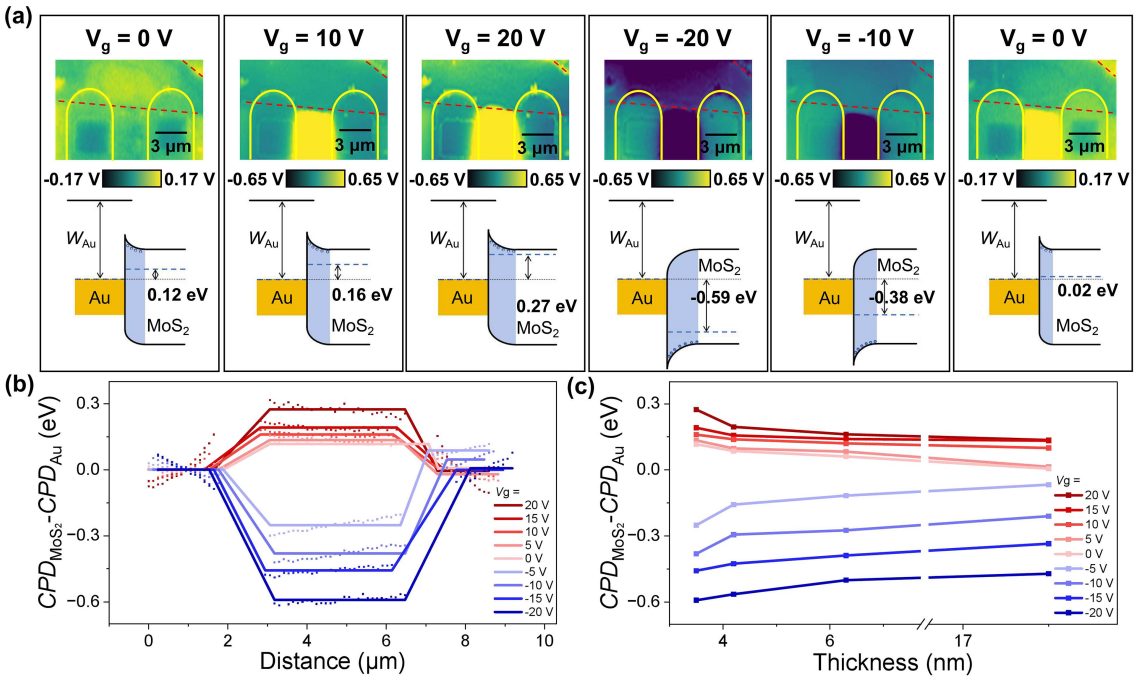

Figure 3 (Color online) Band structure changes of MoS_2 under ferroelectric field modulation. (a) Changes of MoS_2 band under different gate voltages. The top panels show the KPFM surface potential mappings of a five-layer MoS_2 gate-controlled by P(VDF-TrFE) under gate voltages of 0, 10, 20, −20, −10, and 0 V. The first KPFM potential mapping at 0 V gate voltage is the test result without applied voltage. The second KPFM potential mapping at 0 V gate voltage is the data at zero gate voltage during the measurement from −20 to 0 V gate voltage. The selected areas with yellow solid lines and red dashed lines refer to source and drain electrodes, as well as MoS_2. The bottom panels show the band diagrams of MoS_2 at different gate voltages extracted from the KPFM potential maps. The blue dashed line represents the Fermi level of MoS_2. The source and drain electrodes are grounded in the test as a reference for the band position. Under ferroelectric modulation, the band of MoS_2 gradually transitions from n-type to p-type when the gate voltage changes from 20 to −20 V. The scale bars of the figures are all 3 μm. (b) Contact potential difference profile along the source-MoS_2 channel-drain at different gate voltages (from −20 to 20 V in steps of 5 V) with the grounded source and drain electrodes as a reference. The solid points in the figure represent the actual CPD data extracted from the KPFM measurement, and the solid lines represent the calculated average value of CPD. The CPD difference between MoS_2 and Au electrodes shows the Fermi level shift of MoS_2. Under positive gate voltage, the Fermi level gradually shifts upward with the increase of gate voltage, reaching a maximum of nearly 300 meV. Under negative gate voltage, the Fermi level gradually shifts downward with the increase of gate voltage, reaching a maximum of nearly 600 meV. (c) Band variations of MoS_2 with different thicknesses at different gate voltages (from −20 to 20 V in steps of 5 V). The CPD difference between MoS_2 and Au electrodes as a function of gate voltage is shown for four different thicknesses of MoS_2 at 3.5, 4.2, 6.3, and 17.5 nm. The Fermi levels of MoS_2 with different thicknesses under ferroelectric modulation are all significantly shifted with the increase of the gate voltage. Correspondingly, the Fermi level shifts gradually increase with increasing thickness.

dielectric screening leads to a significant decrease in the MoS_2 exciton binding energy, so that a large number of additional excitons can be dissociated into free carriers by the ferroelectric field. In addition, thanks to the high polarization strength D resulting from the high dielectric constant and ferroelectric polarization, P(VDF-TrFE) can achieve significant modulation of the MoS_2 Fermi level. This will be demonstrated in the following. Thus, when the polarization is downward, the Fermi level shifts downward largely, and P(VDF-TrFE) can achieve a large carrier accumulation capability. So, p-type MoS_2 is realized by ferroelectric modulation. The asymmetry of the transfer characteristic curves may originate from the trapping/detrapping process of residual traps at the interface.

The above studies show that a high dielectric constant substrate is beneficial for the realization of p-type MoS_2 transistors, which is particularly important for the integration of MoS_2 in various electronic devices. To deeply reveal the bipolar behavior of MoS_2, we investigated the band changes of MoS_2 at different gate voltages. We measured the surface potential mappings of different thicknesses of MoS_2 modulated by P(VDF-TrFE) ferroelectric field at different gate voltages using KPFM. Using the grounded source and drain electrodes as a reference, we extracted the MoS_2 contact potential difference data ($CPD_{MoS_2} - CPD_{Au}$), which showed the Fermi level shifts of MoS_2 at different gate voltages. Due to the unscreened long-range electrostatic interactions between the conductive probe cantilever and the ferroelectric field, as the gate voltage increases, the overall CPD values of MoS_2 and the source and drain electrodes move upward with a common background. It has been reported that the gate voltage does not affect the local surface potential of the metal electrodes [42–44]; therefore the background signal on the metal electrode surface distinguishes the relative change in the local surface potential from the spatially uniform background ($CPD_{MoS_2} - CPD_{Au}$). This value reflects the effect of the gate voltage on the Fermi level of MoS_2.

We cyclically measured the surface potential changes of MoS_2 between −20 and 20 V with a step size of 5 V.

We selected four different thicknesses of MoS_2, including 3.5, 4.2, 6.3, and 17.5 nm. Fermi level shifts of five-layer MoS_2 extracted from measurement results under gate voltages of 0, 10, 20, −20, −10, and 0 V are given in Figure 3(a) (test results for the remaining layers are shown in Figure S3). MoS_2 Fermi level is 120 meV above the position of Au work function at 0 V. The Fermi level under positive gate voltage gradually shifts upward with increasing gate voltage, indicating the enhanced n-type behavior of the MoS_2 band. The gap between the Fermi level and Au work function position increases to 270 meV at the gate voltage of 20 V. Negative gate voltage produces a larger shift of the Fermi level downward gradually with the increase of the gate voltage, indicating that the MoS_2 band is gradually transformed into p-type. The Fermi level at −20 V gate voltage is lower than the position of Au work function and the gap value reaches 590 meV. At this point, with MoS_2 Fermi level shifting significantly to the valence band and approaching it, hole injection and accumulation are smoothly realized. In addition, due to the effect of remnant polarization, there is a significant shift of the Fermi level after the withdrawal of the gate voltage compared to that before applying the gate voltage. Under downward remanent polarization, the Fermi level is shifted downward by 100 meV relative to the initial. Figure 3(b) shows the $\mathrm{CPD_{MoS_2}} - \mathrm{CPD_{Au}}$ profile along the source-MoS_2 channel-drain at the gate voltage ranging from −20 to 20 V. The MoS_2 Fermi level shift varies from about −600 to 300 meV as V_g goes from −20 to 20 V. The large shift of the Fermi level indicates the strong modulation of the MoS_2 band by the ferroelectric field. While, according to the calculation results given by the band profile, the electric field strength in MoS_2 under positive polarization is much smaller than that under negative polarization, which indicates that the natural n doping of MoS_2 screens the positively polarized field more effectively [41]. This is why the Fermi level shift under negative gate voltage is much larger than that under positive gate voltage. Figure 3(c) shows the band changes of MoS_2 with different thicknesses at different gate voltages. The results show that under ferroelectric modulation, the Fermi levels of MoS_2 with different thicknesses all experience a large shift with increasing gate voltage. However, the shift gradually decreases with the increase in thickness, which originates from the stronger screening of thicker materials against the electric field.

Based on the above research, we further investigated the band structure of MoS_2 homojunction under ferroelectric modulation. The results intuitively showed the n-p band changes of MoS_2 flexibly modulated by ferroelectric field. We used split gates to independently control the polarization states of the left and right sides of the P(VDF-TrFE) ferroelectric gate dielectric, achieving four different configurations of pp, nn, np, and pn, as shown in the left panel of Figure 4(b). When $V_{GL} = V_{GR} = -20$ V (20 V), both sides of the P(VDF-TrFE) are polarized down (up). The device is the pp/nn structure with linear and symmetric output characteristics. With $V_{GL} = -V_{GR} = -20$ V, the left/right side of P(VDF-TrFE) is polarized down/up, forming a pn homogeneous junction with typical rectified output and a current rectification ratio exceeding 10^4. With $V_{GL} = -V_{GR} = 20$ V, the left/right side of P(VDF-TrFE) is polarized up/down and the device is reversed to an np junction.

We conducted KPFM measurement on MoS_2 while applying voltage to G_L and G_R and synchronously tested the state after voltage withdrawal. The device structure and test results are shown in Figure 4(a). The test results with the applied gate voltage are shown in Figure S4. The right figures in Figure 4(a) show the polarized states of pp, pn, np, and nn maintained after the gate voltage is withdrawn from left to right. The results of the contact potential difference (Figure 4(b) left and Figure 4(c)) show that ferroelectric modulation achieves free and flexible n-p band configuration and state retention of the homojunction. When the device forms a pp/nn junction, the left and right MoS_2 Fermi levels shift upward/downward simultaneously. The Fermi level shifts on both sides exhibit good uniformity with a larger downward offset. When the device forms a pn/np junction, the Fermi level of MoS_2 on both sides shifts in opposite directions. The Fermi level of np and pn junctions exhibits good symmetry with a band shift of approximately 240 meV on both sides of the junction. Regarding the issue that the Fermi level change on the p-side of the pp junction is higher than the value of the change in the np or pn junctions, we consider that this difference stems from the weakening of the polarization effect due to the different modulation of the n-type and p-type on both sides of the pn junction. The charge compensation on both sides affects the charge injection of the gate and the electrostatic screening, which, along with the interaction between the opposite polarizations of the gates on both sides, leads to a weakening of the polarization modulation effect in both pn and np junctions. This ultimately leads to different Fermi level shifts in homogeneous junctions. In addition, we performed scanning capacitance microscopy tests on MoS_2 ferroelectric field effect transistors based on P(VDF-TrFE) bottom gate at different gate voltages.

Scanning capacitance microscopy is an electrical AFM imaging technique with nanoscale resolution for analyzing polarity, concentration, and distribution of charge carriers. The SCM technique achieves localized free carrier concentration and type measurements by detecting changes in the sample capacitance signal generated by the modulation of the reference voltage on the free carriers at the sample surface. The phase of the differential capacitance signal ($\mathrm{d}C/\mathrm{d}V$) can be used to identify carrier polarity. The capacitance signal (C) and the amplitude of $\mathrm{d}C/\mathrm{d}V$ can be used to estimate the carrier concentration. The carrier concentration is linearly related to the capacitance signal.

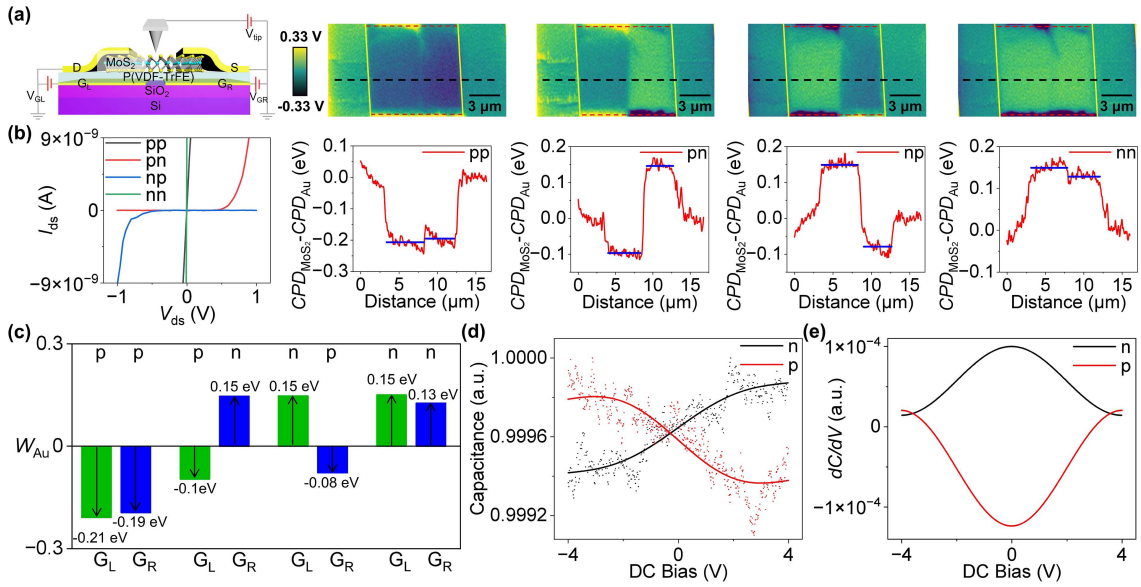

Figure 4 (Color online) MoS_2 homojunction under ferroelectric field modulation. (a) KPFM measurements of MoS_2 homogeneous pn junction with ferroelectric modulation. The left figure is the schematic diagram of measuring the surface potential of the pn junction by KPFM. The device employs P(VDF-TrFE) as the gate dielectric and the split gates (G_L and G_R) beneath the dielectric independently manipulate the ferroelectric domains on the left and right sides. The source and drain electrodes of the device are grounded, and equal positive/negative voltages are applied to the left and right gates with synchronous variations, achieving four different n-p configurations under different ferroelectric polarization states. The figures on the right show the KPFM surface potential maps of the homojunction after different gate voltages were applied and withdrawn. From left to right, they are pp junction ($V_{GL} = V_{GR} = -20$ V), pn junction ($V_{GL} = -V_{GR} = -20$ V), np junction ($V_{GL} = -V_{GR} = 20$ V) and nn junction ($V_{GL} = V_{GR} = 20$ V). The area marked by the yellow solid lines and red dashed lines in the figures is MoS_2. The outer area of the yellow solid lines is the source and drain electrodes. The scale bars in the figure are 3 μm. (b) Electrical characteristics and Fermi level shifts of MoS_2 homojunction under ferroelectric field modulation. The left panel shows the output characteristics of MoS_2 homojunction with different ferroelectric polarization configurations. The output characteristic of the pp/nn junction is linear and symmetric, while the output characteristic of the pn/np junction exhibits typical rectification behavior with a rectification ratio exceeding 10^4. The right panels show the profile of the contact potential difference extracted along the black dashed line in the right figures of (a). The thick blue line in the figure represents the average value of $CPD_{MoS_2} - CPD_{Au}$. Under the pp/nn configuration, the Fermi level on both sides of MoS_2 is shifted in the same direction with good uniformity. Under the pn/np configuration, the Fermi level on both sides is shifted in the opposite direction, exhibiting good symmetry. There is a small jump in the middle of the junction region, which is generated during data processing. There is a certain shift in the junction region potential due to the thermal drift of the instrument. In addition, the incomplete equality of the potential values of the source-drain electrodes on both sides, which originates from a small amount of surface residue and the influence of environmental factors, leads to an incomplete symmetry of the two sides in the data processing, which in turn produces a jump in the junction. (c) Band changes of MoS_2 homojunction under ferroelectric field modulation. The figure shows the Fermi level position of MoS_2 calculated with the work function of Au as a reference. Ferroelectric modulation achieves a freely defined n-p band configuration and retention for the homojunction. The potential barrier height of the np/pn junction is about 240 meV. MoS_2 FeFET charge carriers change measurement by SCM: (d) the C-V curve of MoS_2 obtained from SCM single point measurements at the gate voltage of 20 and -20 V; (e) the dC/dV amplitude curves obtained by derivation. The solid points in the figures represent the actual measurement results, while the solid lines represent the fitting results. n-type (20 V) and p-type (-20 V) MoS_2 exhibit opposite changes in the test results, which intuitively reflects the switching of n-p carriers under ferroelectric modulation.

Figures 4(d) and (e) show the switching of MoS_2 charge carriers at different gate voltages. Under positive gate voltage, the majority of carriers in the n-type semiconductor channel accumulate, the semiconductor capacitance increases, and thus, the capacitance signal is enhanced. Under negative gate voltage, n-type carriers in the channel are depleted and the semiconductor capacitance decreases, so the capacitance signal is weakened. Consequently, the C-V curve shows an increasing trend. Conversely, the C-V curve of p-type semiconductors shows a decreasing trend. Correspondingly, on the dC/dV curve obtained by derivation, the n-type semiconductor has a positive value and the p-type semiconductor has a negative value. Therefore, the polarity of the semiconductor can be recognized by the capacitance signal. In addition, the smaller change in capacitance represents the higher carrier concentration. The single point measurement results of SCM at 20 and -20 V gate voltage visually demonstrate the n-p transition of MoS_2 under ferroelectric modulation (Figures 4(d) and (e)). The changes of MoS_2 capacitance signal and dC/dV phase signal at different gate voltages are respectively shown in Figures S5 and S6. The dC/dV signal changes from a negative to a positive signal when the negative gate voltage turns into the positive gate voltage, indicating that charge carriers transform from p-type to n-type. SCM test results match well with the electrical characteristics of the device and the band change of MoS_2. With the help of SCM, we directly show a smooth switching of MoS_2 between n-type and p-type semiconductors under ferroelectric field modulation.

4 Conclusion

In conclusion, we realized p-type MoS_2 with the help of the significant modulation of the band by high dielectric constant P(VDF-TrFE) ferroelectric film. We quantitatively studied the effects of three different dielectric environments, including Si/SiO_2, hBN, and P(VDF-TrFE), on the band structure and electrical properties of MoS_2 using KPFM. The Fermi level of MoS_2 on the high dielectric constant substrate is significantly shifted. It is worth noting that, unlike MoS_2 field effect transistors on Si/SiO_2 and hBN substrates, MoS_2 ferroelectric field effect transistors with P(VDF-TrFE) bottom gate can exhibit p-type electrical transport behavior. Therefore, we systematically investigated the bipolar behavior and band change of MoS_2 under ferroelectric modulation using in-situ KPFM, thus successfully demonstrating the significant shift of the Fermi level up to nearly 900 meV during the n-p conversion. Finally, we conducted a direct study on the flexible n-p transition of MoS_2 homojunction band under ferroelectric field modulation by combining in-situ KPFM and SCM and explained the p-type modulation of MoS_2 under ferroelectric field. Significant modulation of the MoS_2 band by strong dielectric screening ability and high ferroelectric polarization field of P(VDF-TrFE) is responsible for the ability of MoS_2 to achieve flexible transition between n-p. This work advances the application of MoS_2 in high-performance nanoelectronic devices and provides new opportunities for the development of p-type 2D materials.

Acknowledgements This work was supported by National Key Research and Development Program of China (Grant No. 2024YFA1211500), National Natural Science Foundation of China (Grant Nos. 62025405, 62222413, 62334001, 62405061, 62404232, 62404231), Natural Science Foundation of Shanghai (Grant No. 23ZR1473400), and Department of Science and Technology of Yunnan Province (Grant No. 202402AC080002).

Supporting information Figures S1–S6. The supporting information is available online at info.scichina.com and link.springer.com. The supporting materials are published as submitted, without typesetting or editing. The responsibility for scientific accuracy and content remains entirely with the authors.

References

1 Novoselov K S, Geim A K, Morozov S V, et al. Electric field effect in atomically thin carbon films. Science, 2004, 306: 666–669
2 Xia F, Wang H, Jia Y. Rediscovering black phosphorus as an anisotropic layered material for optoelectronics and electronics. Nat Commun, 2014, 5: 4458
3 Buscema M, Groenendijk D J, Blanter S I, et al. Fast and broadband photoresponse of few-layer black phosphorus field-effect transistors. Nano Lett, 2014, 14: 3347–3352
4 Radisavljevic B, Radenovic A, Brivio J, et al. Single-layer MoS_2 transistors. Nat Nanotech, 2011, 6: 147–150
5 Fang H, Chuang S, Chang T C, et al. High-performance single layered WSe_2 p-FETs with chemically doped contacts. Nano Lett, 2012, 12: 3788–3792
6 Yan H, Zhao Q, Chen Y, et al. $MoTe_2/SnSe_2$ tunneling diode regulated by giant ferroelectric field. IEEE Trans Electron Devices, 2023, 70: 5966–5971
7 Chen Y, Wang X, Huang L, et al. Ferroelectric-tuned van der Waals heterojunction with band alignment evolution. Nat Commun, 2021, 12: 4030
8 Wu S, Chen Y, Wang X, et al. Ultra-sensitive polarization-resolved black phosphorus homojunction photodetector defined by ferroelectric domains. Nat Commun, 2022, 13: 3198
9 Tai X, Chen Y, Wu S, et al. High-performance ReS_2 photodetectors enhanced by a ferroelectric field and strain field. RSC Adv, 2022, 12: 4939–4945
10 Chen Y, Wang X, Wu G, et al. High-performance photovoltaic detector based on $MoTe_2/MoS_2$ van der Waals heterostructure. Small, 2018, 14: 1703293
11 Chen Y, Yin C, Wang X, et al. Multimode signal processor unit based on the ambipolar WSe_2-Cr Schottky junction. ACS Appl Mater Interfaces, 2019, 11: 38895–38901
12 Wang H T, Wu S Q, Chen Y, et al. Bulk photovoltaic effect in two-dimensional ferroelectric α-In_2Se_3. Sci China Inf Sci, 2025, 68: 122401
13 Qiu H, Yu Z H, Zhao T G, et al. Two-dimensional materials for future information technology: status and prospects. Sci China Inf Sci, 2024, 67: 160400
14 Wu Z, Lyu Y, Zhang Y, et al. Large-scale growth of few-layer two-dimensional black phosphorus. Nat Mater, 2021, 20: 1203–1209
15 Liu B, Köpf M, Abbas A N, et al. Black Arsenic-Phosphorus: layered anisotropic infrared semiconductors with highly tunable compositions and properties. Adv Mater, 2015, 27: 4423–4429
16 Liu S Y, Xiong X, Wang X, et al. Hole mobility enhancement in monolayer WSe_2 p-type transistors through molecular doping. Sci China Inf Sci, 2024, 67: 160406
17 Raja A, Chaves A, Yu J, et al. Coulomb engineering of the bandgap and excitons in two-dimensional materials. Nat Commun, 2017, 8: 15251
18 Utama M I B, Kleemann H, Zhao W, et al. A dielectric-defined lateral heterojunction in a monolayer semiconductor. Nat Electron, 2019, 2: 60–65
19 Ouyang Y, Jiang Z, Ulstrup S, et al. Enhancing MoS_2 electronic performance with solid-state lithium-ion electrolyte contacts through dielectric screening. ACS Nano, 2024, 18: 33310–33318

20 Luo P, Zhuge F, Zhang Q, et al. Doping engineering and functionalization of two-dimensional metal chalcogenides. Nanoscale Horiz, 2019, 4: 26–51

21 Mak K F, Lee C, Hone J, et al. Atomically thin MoS_2: a new direct-gap semiconductor. Phys Rev Lett, 2010, 105: 136805

22 Imran A L, He X, Liu J W, et al. Highly responsive broadband Si-based MoS_2 phototransistor on high-k dielectric. Sci China Inf Sci, 2024, 67: 160403

23 Das S, Chen H Y, Penumatcha A V, et al. High performance multilayer MoS_2 transistors with scandium contacts. Nano Lett, 2013, 13: 100–105

24 Zhang Y, Ye J, Matsuhashi Y, et al. Ambipolar MoS_2 thin flake transistors. Nano Lett, 2012, 12: 1136–1140

25 Chen Y, Wang X, Wang P, et al. Optoelectronic properties of few-layer MoS_2 FET gated by ferroelectric relaxor polymer. ACS Appl Mater Interfaces, 2016, 8: 32083–32088

26 Wang X, Wang P, Wang J, et al. Ultrasensitive and broadband MoS_2 photodetector driven by ferroelectrics. Adv Mater, 2015, 27: 6575–6581

27 Wang X, Liu C, Chen Y, et al. Ferroelectric FET for nonvolatile memory application with two-dimensional $MoSe_2$ channels. 2D Mater, 2017, 4: 025036

28 Li D, Wang X, Chen Y, et al. The ambipolar evolution of a high-performance WSe_2 transistor assisted by a ferroelectric polymer. Nanotechnology, 2018, 29: 105202

29 Wang X, Chen Y, Wu G, et al. Graphene Dirac point tuned by ferroelectric polarization field. Nanotechnology, 2018, 29: 134002

30 Wu S Q, Wang X D, Jiang W, et al. Interface engineering of ferroelectric-gated MoS_2 phototransistor. Sci China Inf Sci, 2021, 64: 140407

31 Kutrowska-Girzycka J, Zieba-Ostój E, Biegańska D, et al. Exploring the effect of dielectric screening on neutral and charged-exciton properties in monolayer and bilayer $MoTe_2$. Appl Phys Rev, 2022, 9: 041410

32 Cho Y, Berkelbach T C. Environmentally sensitive theory of electronic and optical transitions in atomically thin semiconductors. Phys Rev B, 2018, 97: 041409

33 Castellanos-Gomez A, Cappelluti E, Roldán R, et al. Electric-field screening in atomically thin layers of MoS_2: the role of interlayer coupling. Adv Mater, 2013, 25: 899–903

34 McDonnell S, Addou R, Buie C, et al. Defect-dominated doping and contact resistance in MoS_2. ACS Nano, 2014, 8: 2880–2888

35 Chen R S, Ding G, Zhou Y, et al. Fermi-level depinning of 2D transition metal dichalcogenide transistors. J Mater Chem C, 2021, 9: 11407–11427

36 Chuang S, Battaglia C, Azcatl A, et al. MoS_2 P-type transistors and diodes enabled by high work function MoO_x contacts. Nano Lett, 2014, 14: 1337–1342

37 Lee C, Rathi S, Khan M A, et al. Comparison of trapped charges and hysteresis behavior in hBN encapsulated single MoS_2 flake based field effect transistors on SiO_2 and hBN substrates. Nanotechnology, 2018, 29: 335202

38 Khakbaz P, Driussi F, Giannozzi P, et al. Engineering of metal-MoS_2 contacts to overcome Fermi level pinning. Solid-State Electron, 2022, 194: 108378

39 Song E B, Lian B, Kim S M, et al. Robust bi-stable memory operation in single-layer graphene ferroelectric memory. Appl Phys Lett, 2011, 99: 042109

40 Lipatov A, Fursina A, Vo T H, et al. Polarization-dependent electronic transport in graphene/$Pb(Zr,Ti)O_3$ ferroelectric field-effect transistors. Adv Elect Mater, 2017, 3: 1700020

41 Sun X, Chen Y, Zhao D, et al. Measuring band modulation of MoS_2 with ferroelectric gates. Nano Lett, 2023, 23: 2114–2120

42 Yu Y J, Zhao Y, Ryu S, et al. Tuning the graphene work function by electric field effect. Nano Lett, 2009, 9: 3430–3434

43 Wang Z, Li Q, Chen Y, et al. The ambipolar transport behavior of WSe_2 transistors and its analogue circuits. NPG Asia Mater, 2018, 10: 703–712

44 Li Y, Xu C Y, Zhang B Y, et al. Work function modulation of bilayer MoS_2 nanoflake by backgate electric field effect. Appl Phys Lett, 2013, 103: 033122